Exchange bias induced by the Fe$_3$O$_4$ Verwey transition

J. de la Venta,[1,*] M. Erekhinsky,[1] Siming Wang,[1,2] K. G. West,[1] R. Morales,[3,4] and Ivan K. Schuller[1]

[1]*Department of Physics and Center for Advanced Nanoscience, University of California San Diego, La Jolla, California 92093, USA*
[2]*Materials Science and Engineering Program, University of California San Diego, La Jolla, California 92093, USA*
[3]*Departamento de Química-Física, Universidad del País Vasco, 48940 Leioa, Spain*
[4]*IKERBASQUE, Basque Foundation for Science, 48011 Bilbao, Spain*

We present a study of exchange bias in different configurations of V$_2$O$_3$ thin films with ferromagnetic layers. The exchange bias is accompanied by a large vertical shift in magnetization. These effects are only observed when V$_2$O$_3$ is grown on top of Ni$_{80}$Fe$_{20}$ permalloy. The magnitude of the vertical shift is as large as 60% of the total magnetization, which has never been reported in any system. X-ray diffraction studies show that the growth conditions promote the formation of a ferrimagnetic Fe$_3$O$_4$ interlayer. The change in the easy magnetization axis of Fe$_3$O$_4$ across the Verwey transition at 120 K is correlated with the appearance of exchange bias and vertical shift in magnetization. Both phenomena disappear above 120 K, indicating a direct relationship between the magnetic signature of the Verwey transition and the exchange bias.

PACS number(s): 75.70.−i, 75.30.Et, 75.60.−d

I. INTRODUCTION

Exchange bias (EB),[1,2] the horizontal shift of the hysteresis loop in ferromagnetic/antiferromagnetic (or ferrimagnetic) systems, is one of the most studied effects in thin film magnetism and is the basis for several applications.[3,4] Most studies of EB in thin films were done by growing ferromagnetic (FM) layers on top of antiferromagnetic (AFM) oxides. These oxides exhibit unique properties, including collective phenomena such as magnetism, ferroelectricity, superconductivity, metal–insulator transitions, enhanced photoconductivity, and electron transfer.[5–10] These materials hold great potential for revolutionary developments, which may arise from the manipulation and control of novel emergent properties that are not present in ordinary semiconductors or metals. Interesting possibilities arise when FM thin films are layered with transition metal oxides that undergo a structural transition where there is a change in resistivity and magnetic properties. This transition provides an external tuning capability of the properties by changing the temperature. It affords a unique opportunity to study EB not only when the materials are cooled through the Neel temperature but also when their structure and resistivity change across the transition.

A particularly interesting class of oxides is the vanadium oxides VO$_x$[11–13] system. Among these phases, vanadium sesquioxide, V$_2$O$_3$, undergoes a first-order metal–insulator transition at $T = 160$ K from a low-temperature AFM insulating phase to a high-temperature paramagnetic metallic phase.[14–16] The crystal structure changes from monoclinic in the insulating phase to rhombohedral symmetry in the metallic phase. Electronic and structural properties of V$_2$O$_3$ thin films epitaxially grown on different sapphire (α-Al$_2$O$_3$) planes have been extensively studied.[17,18] Although the phase diagram[16] suggests that a reduction in the metal–insulator transition may occur for some strain values, Allimi *et al.*[18] showed how the transition temperatures of V$_2$O$_3$ films grown on (11$\bar{2}$0) a- and (0001) c-plane sapphire substrates were enhanced.

The aim of this work is to study EB in V$_2$O$_3$ with different FM thin films. For this purpose, different combinations of FM and AFM (V$_2$O$_3$) layers have been grown on (1$\bar{1}$02) r-plane

sapphire. EB has previously been observed in bilayers of V$_2$O$_3$ grown on (11$\bar{2}$0) a-plane sapphire substrates with Co on top.[19] However, EB is absent when the top layer is Fe, which was attributed to the presence of a magnetically "dead" Fe layer at the interface. Additional investigations of Co, Ni, and Fe on top of V$_2$O$_3$ grown on (0001) c-plane and (11$\bar{2}$0) a-plane sapphire substrates[20] found EB for all combinations except Fe on V$_2$O$_3$ (11$\bar{2}$0).

Here, we report the observation of substantial EB in permalloy (Py)/V$_2$O$_3$ bilayers with a large vertical shift in magnetization never before observed in any system. From a series of well-defined experiments—(1) x-ray diffraction, (2) magnetization and magnetotransport, (3) Cl$_2$ plasma etch, (4) annealing, (5) trilayer, and (6) (Ni)/V$_2$O$_3$ and (Py)/V$_2$O$_3$ bilayers—we show that the formation of a Fe$_3$O$_4$ interfacial layer produces the EB and the vertical shift in the FM magnetization. The results imply that the change in the easy magnetization axis occurring at the Fe$_3$O$_4$ Verwey transition is responsible for the vertical shift in the FM magnetization and EB.

II. EXPERIMENTAL DETAILS

The samples were prepared in a high-vacuum sputtering deposition system with a base pressure of 1×10^{-7} Torr using ultrahigh-purity argon sputtering gas. The pressure during the deposition was 4×10^{-3} Torr. Bilayers and trilayers were deposited by radiofrequency (RF) sputtering of Ni$_{80}$Fe$_{20}$, Ni, and V$_2$O$_3$ targets on r-plane sapphire (1$\bar{1}$02) substrates. The different configurations are shown in Fig. 1. The RF magnetron power was kept at 100 W. For the FM/V$_2$O$_3$ bilayer [Fig. 1(a) and 1(b)], the FM layer was deposited at room temperature. Next, the temperature was increased to 750 °C at 7 °C/min and the V$_2$O$_3$ layer was deposited. Finally, the sample was cooled to room temperature at 7 °C/min. For the V$_2$O$_3$/FM bilayer [Fig. 1(c)], the V$_2$O$_3$ layer was deposited at 750 °C. After cooling the sample to room temperature, the FM layer was deposited. Samples with different thicknesses for FM layers (20–60 nm) and V$_2$O$_3$ (25–100 nm) were fabricated. For the FM/V$_2$O$_3$/FM trilayers [Fig. 1(d)], the two bottom layers were deposited as explained for the FM/V$_2$O$_3$ bilayers and the top
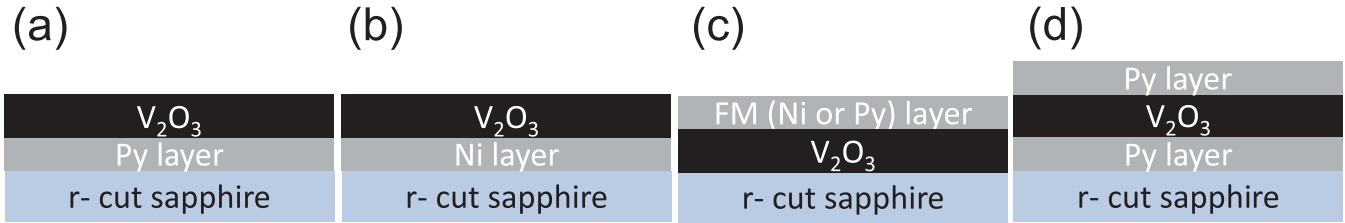
FIG. 1. (Color online) Schematic model of different samples studied. (a) and (b) Py or Ni was deposited at room temperature. The V_2O_3 layer was deposited later at 750 °C after a 7 K/min heating ramp. (c) The V_2O_3 layer was deposited at 750 °C and the top FM at room temperature. (d) Trilayer used for MOKE measurements.

FM was deposited using two conditions: at room temperature and at 750 °C.

X-ray diffraction was performed with a Bruker D8 Discovery rotating anode x-ray diffractometer using Cu Kα radiation.

Magnetic characterization was performed using a superconducting quantum interference device magnetometer (SQUID) and the magneto-optical Kerr effect (MOKE). While MOKE is only sensitive to the surface magnetization (the penetration length of the light is less than 50 nm for the FM layer) the SQUID measures the full magnetic moment of the sample. The samples were cooled from 250 to 10 K in different cooling fields. Hysteresis loops were measured at various temperatures after each field cooling.

In addition, the magnetoresistance (MR) of Py/V_2O_3 bilayers were measured on 40-μm-wide bars etched out of the whole film using standard photolithographic techniques. Because the resistivity of V_2O_3, even in the metallic phase, is much higher than the resistivity of the FM layer, the majority of the current in the film flows through the FM metal layers. Therefore, the anisotropic MR reflects the switching fields of the FM layer.

III. RESULTS AND DISCUSSION

A. X-ray diffraction

The x-ray diffraction of FM/V_2O_3 bilayers [Fig. 1(a) and 1(b)] shows the following diffraction peaks [Fig. 2]: Py or Ni in the (111) direction and V_2O_3 in the (001) direction. The Py/V_2O_3 bilayers [Fig. 1(a)] exhibit a series of unexpected diffraction peaks (with instrumentally limited widths), marked as dots in Fig. 2. Two possible candidates match the x-ray diffraction peaks for this unexpected phase: V_3O_4 (111) or magnetite Fe_3O_4 (111), both with the same cubic $Fd-3m$ structure. The peak positions for (111) family planes of bulk Fe_3O_4 (or V_3O_4) are marked as lines at the top of Fig. 2. These unexpected diffraction maxima did not appear when the V_2O_3 thin film is deposited on top of a Ni layer. A literature review indicates that the existence of the V_3O_4 phase is uncertain. This was claimed only twice in the literature: ultrathin, less than 1 monolayer,[21] or V_3O_4 spinel phase generated from V_2O_5 by compressive shock waves stabilized by an Fe admixture.[22]

B. Magnetization and magnetotransport

Surprisingly, only the Py/V_2O_3 bilayers [Fig. 1(a)] showed an EB field with a large vertical shift in magnetization (M_{Shift}; Fig. 3). Both EB and M_{Shift} vanish above 120 K. No EB was found in Ni/V_2O_3 bilayers [Fig. 1(b)]. In addition, bilayers with the reverse configuration, i.e., V_2O_3 at the bottom and

FM (Py or Ni) on top [Fig. 1(c)], show no EB. Hence, the presence of EB is related to an interaction between the bottom Py layer and the top V_2O_3 thin film.

The most striking effect is the large vertical shift, up to 60% of the total magnetization at 10 K, for Py (30 nm)/V_2O_3 (100 nm), as shown by black triangles in Fig. 4. Such large magnetization shifts were never reported in any system. In FeF_2-Fe bilayers, the shift of the hysteresis loop is ~1% of the total magnetization.[23] X-ray magnetic circular dichroism shows a small vertical offset in Co/$Ir_{20}Mn_{80}$ bilayers, indicating that only 7% of the total uncompensated moments were pinned.[24] Larger values have been recently reported in other systems.[25,26] The large vertical shift in the Py/V_2O_3 bilayers indicates the presence of a large number of pinned spins. The influence of the field cooling has been investigated at fields of up to 5 T. In all cases, the shift of the hysteresis loop is "upward" for positive cooling fields. No dependence of M_{Shift} on the magnitude of the cooling field or indication of positive
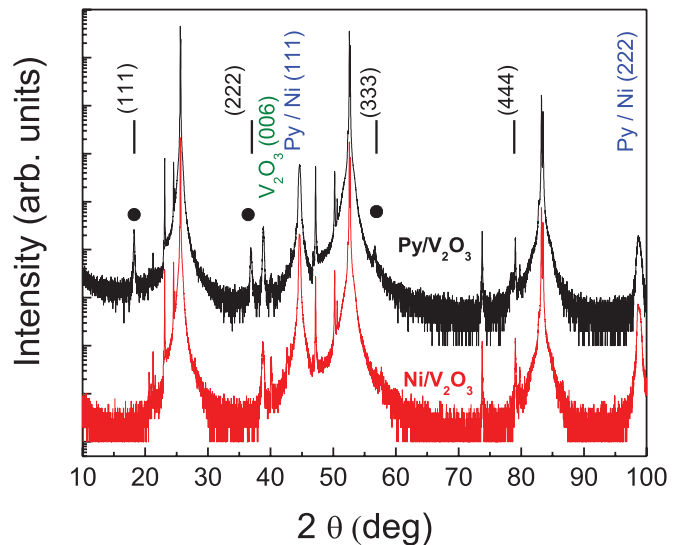

FIG. 2. (Color online) X-ray diffraction patterns for two bilayers: Py (30 nm)/V_2O_3 (100 nm) (top black) and Ni (30 nm)/V_2O_3 (100 nm) (bottom red). Diffraction maxima from Py or Ni (111) and from V_2O_3 (006) are marked in the figure; diffraction maxima shown by the black dots are from an unexpected phase. Peak positions from Fe_3O_4 or V_3O_4 (111) planes are marked at the top. All other diffraction maxima not marked in the figure are due to the r-cut sapphire substrate. The (444) peak overlaps with one of the substrate peaks. See supplementary material for the substrate x-ray diffraction pattern.
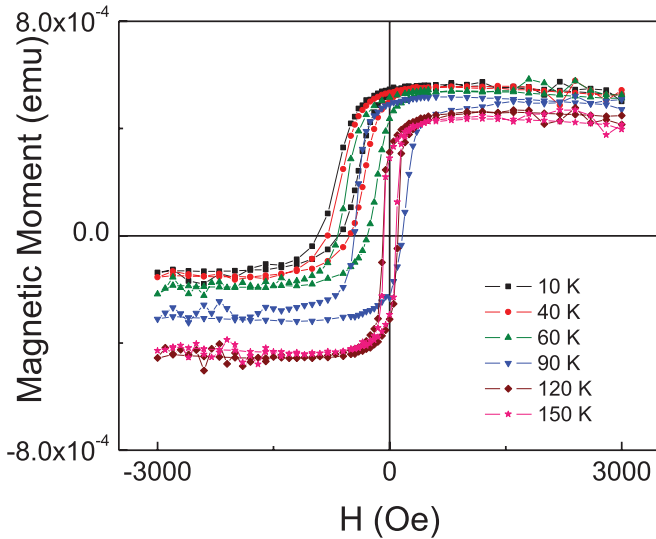
FIG. 3. (Color online) Hysteresis loops at different temperatures in Py (30 nm)/V$_2$O$_3$ (100 nm) bilayers. The sample was cooled from room temperature to 10 K with a field of 1000 Oe.

EB was found. These findings imply that the coupling between the different layers is FM.[23] Samples with 25 nm of V$_2$O$_3$ show no EB or M_{Shift}, as indicated by the red squares in Fig. 4.

The MR measurements of Py (30 nm)/V$_2$O$_3$ (50 nm) bilayers confirmed the presence of EB in samples containing Py/V$_2$O$_3$ interfaces. After the samples were cooled to 4.2 K in the 1000 Oe positive magnetic field, the MR was measured at different monotonically increasing temperatures. Figure 5 shows the H field dependence of resistance at different temperatures. For each temperature, there are two curves corresponding to different magnetic field sweep directions.
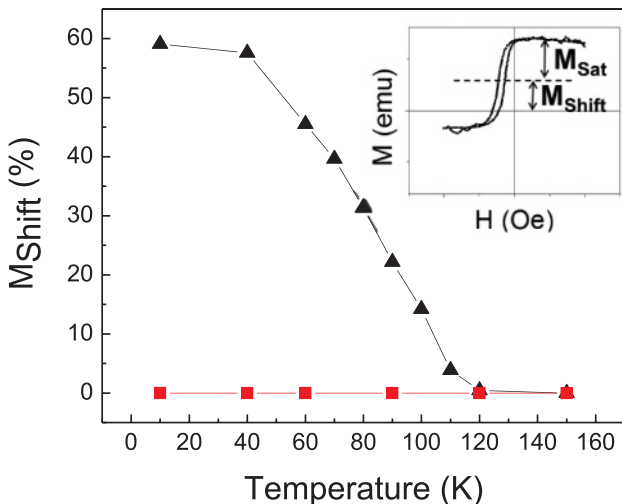

FIG. 4. (Color online) M_{Shift} values as a function of the temperature for bilayers of different thicknesses, Py (30 nm)/V$_2$O$_3$ (y): 100 nm (black triangles) and 25 nm (red squares). M_{Shift} is absent for the 25-nm V$_2$O$_3$ film. The cooling field value was 1000 Oe. In the inset, M_{Shift} (%) has been calculated from the shift of the loop with respect to the abscissa axis and normalized to the values of the saturation M_{Sat} at positive fields.

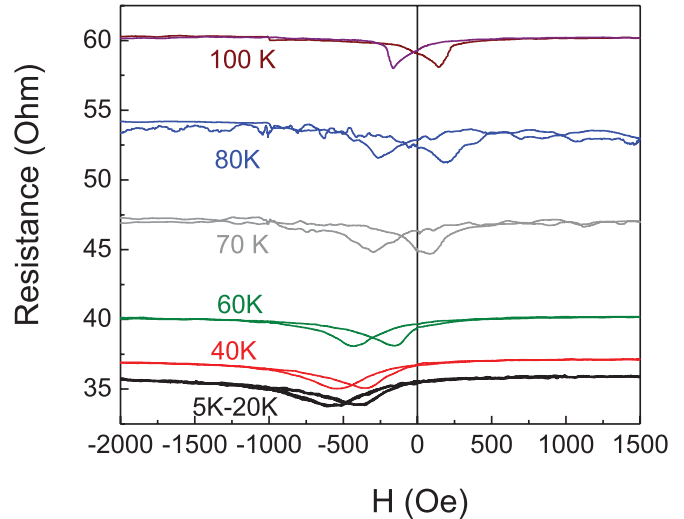FIG. 5. (Color online) MR measurements at different temperatures in Py (30 nm)/V$_2$O$_3$ (50 nm). The sample was cooled from 300 to 4.2 K with an applied field of 1000 Oe.

Below 100 K, the MRs are centered on a nonzero field, indicating the presence of EB. As the magnetic field is swept from a positive to negative (or vice versa), the distance between minima in the MR indicates the coercivity of the FM layer. At 5 and 20 K, the curves match, giving the same values of EB. At 100 K, the bilayer MR is almost symmetric around the zero field and the midpoint of the MR gradually shifts toward the negative field. This indicates that the blocking temperature obtained from the MR is ~100 K.

The temperature dependences of the exchange bias (H_{EB}) and coercivity (H_C) for 30 nm of Py and different V$_2$O$_3$ thicknesses are plotted in Fig. 6. Here, H_{EB} and H_C extracted from SQUID and MR measurements are in good quantitative agreement for Py (30 nm)/V$_2$O$_3$ (50 nm), as shown by the solid and empty circles in Fig. 6. In addition, H_{EB} and H_C are slightly larger for the bilayer with a thicker V$_2$O$_3$ film (100 nm), indicating that it is not only caused by a surface effect.[27] The blocking temperature, i.e., the temperature at which EB disappears, is 120 K in all cases. When the thickness of the V$_2$O$_3$ layer is 25 nm, neither M_{Shift} nor EB was observed (red squares in Figs. 4 and 6, respectively).

C. Cl$_2$ plasma etch

To investigate the cause of EB and clarify the origin and composition of the unexpected phase found from x-ray diffraction (Fig. 2), one of the samples was subjected to reactive ion etching. The Cl$_2$ plasma quickly etches vanadium and its oxides but not Py. The V$_2$O$_3$ (006) x-ray diffraction peaks disappear after etching (Fig. 7), whereas the diffraction maxima arising from the new phase remain. After etching, EB was still present with H_{EB} and M_{Shift} as in the virgin samples. This indicates that the unexpected phase is Fe$_3$O$_4$ rather than V$_3$O$_4$.

D. Annealing

Figure 8(a) shows the diffraction maxima 36.86° from Fe$_3$O$_4$ (222) and 38.84° from V$_2$O$_3$ (006). Figure 8(b) shows
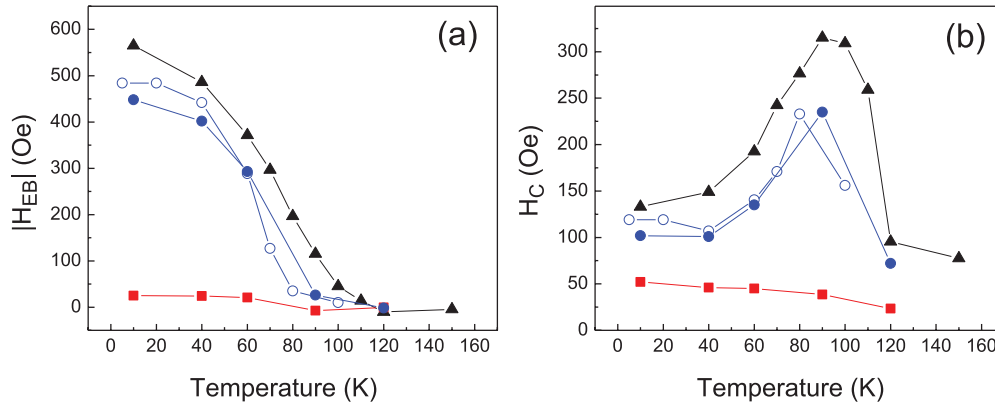
FIG. 6. (Color online) (a) Dependence of the EB field with temperature. (b) Dependence of the coercive field with temperature. Py (30 nm)/V$_2$O$_3$ (100 nm) bilayers are measured with SQUID (solid black triangles), Py (30 nm)/V$_2$O$_3$ (50 nm) is measured with SQUID (solid blue circles), Py (30 nm)/V$_2$O$_3$ (50 nm) is from MR measurements (open blue circles), and Py (30 nm)/V$_2$O$_3$ (25 nm) is measured with SQUID (solid red squares).

the peaks 44.6° from Py (111). Bilayers with 30-nm Py and different thicknesses of V$_2$O$_3$ are included. For better visualization, the x-ray data have been smoothed, and the x-ray diffraction intensity in Fig. 8(a) is plotted in the linear scale, whereas in Fig. 8(b) the vertical scale is logarithmic. (For raw data, see supplementary material.[28])

The Py (30 nm)/V$_2$O$_3$ (25 nm) bilayer, which did not show M_{Shift} or EB (red squares in Figs. 4 and 6, respectively) shows V$_2$O$_3$ (006) x-ray diffraction peaks but not those from the unexpected phase [Fig. 8(a)]. Hereafter, we refer to this sample as the unreacted bilayer. As an additional test, this bilayer was subjected to thermal treatment. After depositing the 25-nm V$_2$O$_3$ layer on top of Py for 6 min and 15 s, the

temperature was kept at 750 °C for additional 18 min 45 s. The 25 min total time at 750 °C is the same as the deposition time for 100-nm V$_2$O$_3$. After this annealing, both the new diffraction maxima [Fig. 8(a)] and EB appeared. The short deposition time (6 min 15 s) for a 25-nm V$_2$O$_3$ sample is not enough to produce the interface reaction, giving rise to the Fe$_3$O$_4$ interfacial layer. However, stopping the deposition but maintaining the temperature provides the conditions for Fe$_3$O$_4$ layer formation. The Fe$_3$O$_4$ (222) peaks in the samples with 50- and 100-nm V$_2$O$_3$ have the same intensity and sharpness. This is an additional indication that the thickness of the Fe$_3$O$_4$ layer is similar in both cases. As expected, the peak from V$_2$O$_3$ (006) has a higher intensity in 100 nm of V$_2$O$_3$. The intensity from the 38.84° peak for the unreacted bilayer indicates that the V$_2$O$_3$ thickness is between those of bilayers with 50 and 100 nm of V$_2$O$_3$.

The peaks close to 44.5° [Fig. 8(b)] provide further clues regarding the interface reaction of the Py film. In all bilayers, the peak position shifts (gradually) toward higher angles (44.6° and 44.63°) and away from the unreacted bilayer (44.38°). The corresponding lattice parameters are 3.5124, 3.5147, and 3.5312 Å. The latter is closer to the Py bulk value of 3.5507 Å, while the first are closer to the bulk Ni value of 3.5238 Å. The finite size Laue oscillations around the Bragg peak for the unreacted sample are more intense and clearer than the ones of the reacted samples, indicating that the interfaces are sharper. The finite size oscillations imply that the Py thickness is 28 nm for the unreacted bilayer as opposed to 23–24 nm for the rest of the samples. Thus, the Py thickness is reduced ~5 nm by the reaction, and the unreacted sample shows a smoother Py surface and lattice parameters closer to bulk Py. When the reaction to form Fe$_3$O$_4$ takes place, the surfaces become rougher and the lattice parameter changes closer to bulk Ni. All of this suggests Fe migration from Py to form the Fe$_3$O$_4$ layer.
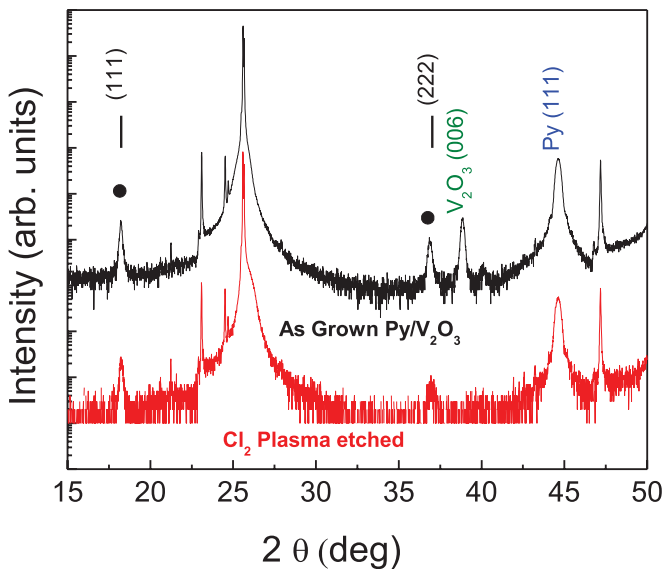

FIG. 7. (Color online) X-ray diffraction patterns for a bilayer Py (30 nm)/V$_2$O$_3$ (100 nm) as grown (top black) and after etching (bottom red). Diffraction maxima from V$_2$O$_3$ and Py are labeled in the figure; diffraction maxima shown by the black dots are from an unexpected phase. Peak positions from Fe$_3$O$_4$ (111) planes are marked at the top. All other diffraction maxima not marked in the figure are due to the r-cut sapphire substrate.

E. Trilayers

MOKE measurements on Py (30 nm)/V$_2$O$_3$ (100 nm)/Py (30 nm) trilayers [Fig. 1(d)] grown on double-sided, polished
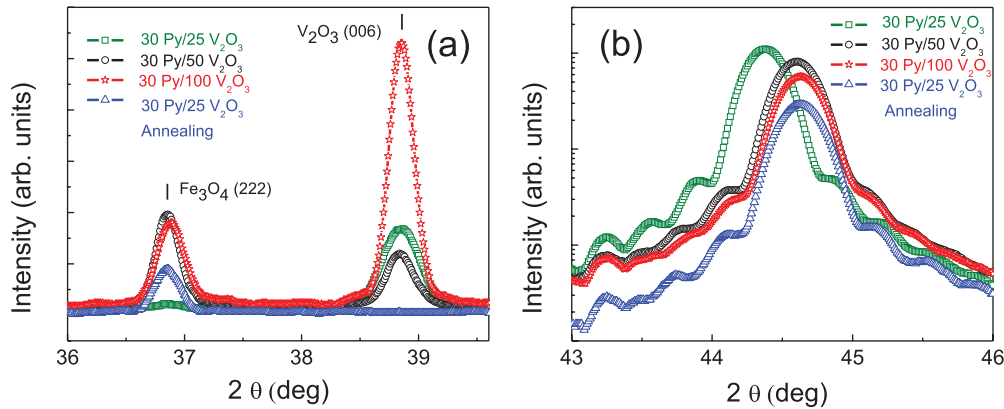
FIG. 8. (Color online) X-ray diffraction patterns focused around the maxima from: (a) Fe$_3$O$_4$ (222) and V$_2$O$_3$ (006) and (b) Py (111): 30-nm Py/25-nm V$_2$O$_3$ (open green squares), 30-nm Py/50-nm V$_2$O$_3$ (open black circles), 30-nm Py/100-nm V$_2$O$_3$ (open red stars), and 30-nm Py/25-nm V$_2$O$_3$ annealed (open blue triangles). Fe$_3$O$_4$ (222) is located at 36.86°, V$_2$O$_3$ (006) is at 38.84°, and Py peaks shift from 44.38° to 44.6° and 44.63°.

sapphire are shown in Fig. 9. MOKE measurements are only sensitive to surface magnetization, because the light penetration length in the FM layer is ~50 nm. MOKE is not a measure of the absolute M value, so it can only confirm the presence of the EB field—not the vertical shift in the magnetic moment. In agreement with the previous ideas, EB is only found in the bottom layer (Fig. 9). As a further check, EB is absent for the top Py layer deposited at room temperature or even at 750 °C. Thus, the Fe$_3$O$_4$ (111) interface is created when V$_2$O$_3$ is deposited on top of Py.

Although the top Py layer exhibits no EB independent of the deposition temperature, its properties are different when deposited at room temperature from when deposited at 750 °C. For room temperature deposition, the top layer has the characteristic metallic shiny aspect of metals. In contrast, the surface becomes opaque at a higher temperature; thus, the reflected laser intensity is somewhat reduced and the MOKE signal is nosier [Fig. 9(b)]. Moreover, the coercive field of this top layer is smaller for room temperature deposition [Fig. 9(b)], which also implies smoother interfaces. The x-ray diffraction data (see supplementary material[28])

shows that the Fe$_3$O$_4$ and V$_2$O$_3$ interlayers are formed when the top layer is deposited either at room temperature or at 750 °C.

F. Discussion

All the extensive experimental evidence discussed previously shows that an unexpected interfacial phase is formed by interfacial diffusion or reaction. Three timescales are relevant. The first is short deposition times, without Fe$_3$O$_4$ formation. Py preserves its bulklike characteristics, the surfaces are smoother [Fig. 8(b)], and V$_2$O$_3$ deposited on top of Py "survives." This final point also explains why the V$_2$O$_3$ peak intensities are larger for 25-nm V$_2$O$_3$ than for 50-nm V$_2$O$_3$. Second, intermediate deposition times cause an interface reaction between Py and V$_2$O$_3$ to form the Fe$_3$O$_4$ layer. The Py lattice parameter changes closer to bulk Ni, and the interfaces become rougher. A process similar to medium deposition times occurs when annealing the samples for longer periods after deposition. In this case, the 25-nm V$_2$O$_3$ layer is destroyed during the process [Fig. 8(a)], giving rise to the formation
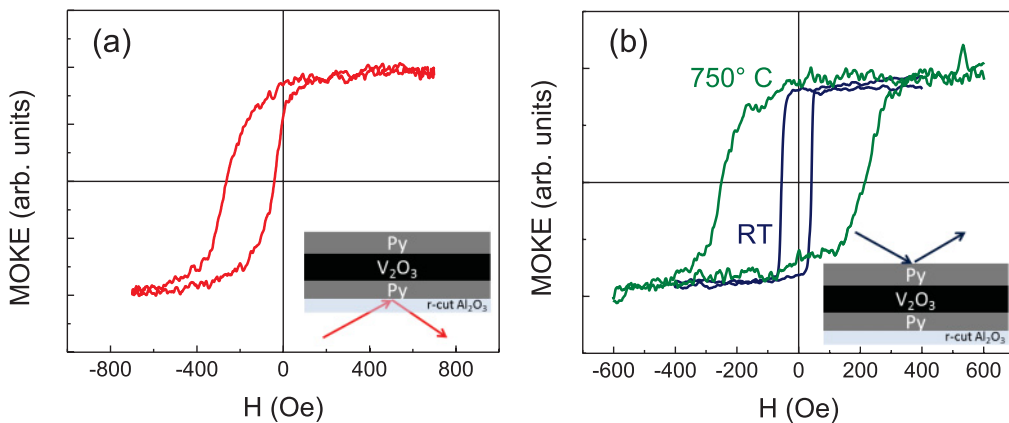

FIG. 9. (Color online) MOKE hysteresis loops at 10 K after cooling the sample, with a field of 1000 Oe. (a) MOKE probing the bottom Py layer. (b) MOKE probing the top Py layer deposited at room temperature and at 750 °C. Insets show MOKE probing each FM individual layer.
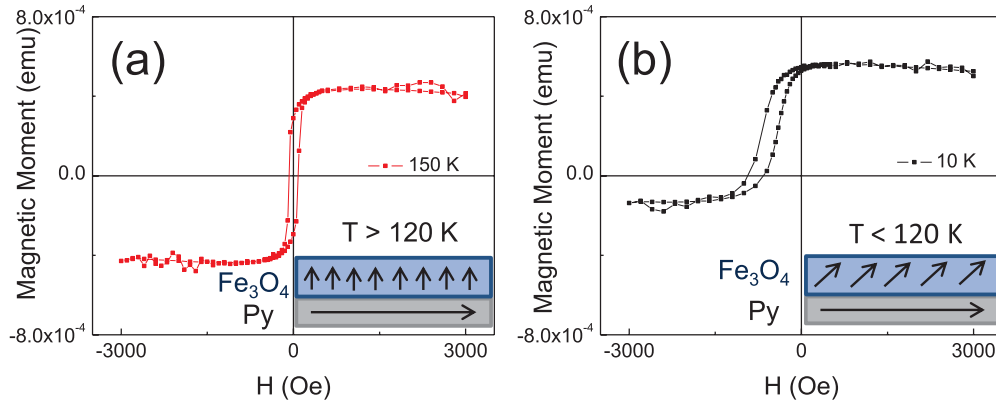
FIG. 10. (Color online) Hysteresis loops in Py (30 nm)/V_2O_3 (100 nm) bilayers after field cooling at (a) 150 K and (b) 10 K. Insets show the simplified magnetization easy-axis configuration of the Py/Fe_3O_4 bilayer: (a) [111] above the transition and (b) [100] and below the transition.

of Fe_3O_4. Finally, there are longer deposition time. After the reaction takes place, the Fe_3O_4 and Py thicknesses and their lattice parameters are stable, and V_2O_3 continues growing on the newly formed Fe_3O_4.

All magnetic data are consistent with EB and M_{Shift} being caused by the magnetic interaction between the Py and an interfacial Fe_3O_4. As further evidence, when V_2O_3 is deposited on a Ni layer, neither the EB nor the presence of the new Fe_3O_4 phase was found.

Fe_3O_4 is a ferrimagnetic material with a Curie temperature of 825 K that changes lattice symmetry and exhibits a metal–insulator transition $\sim$120 K (T_v), the Verwey transition.[29,30] The change in crystal structure is accompanied by magnetization changes. The blocking temperature for EB found here coincides with the Fe_3O_4 Verwey transition and is substantially lower than the 160-K AFM transition of V_2O_3 as shown in Fig. 6(a). This again indicates that EB and M_{Shift} vanishing above 120 K should be attributed to the Fe_3O_4 Verwey transition. Earlier measurements using magnetite Fe_3O_4 showed EB that vanishes at 200 and 275 K because of antiphase boundaries[31] and a spin-glass–like phase,[32] respectively. FM/Fe_3O_4 bilayers showed EB,[33,34] with smaller values of H_{EB} and no M_{Shift} without indications of a blocking temperature. On the other hand, EB found in AFM/Fe_3O_4 bilayers is attributed to presence of the AFM phase.[35,36] To the best of our knowledge, this is the first direct observation of EB that is correlated with the appearance of the Verwey transition in Fe_3O_4.

Although the Verwey transition has been known for more than 70 years, its origin is still controversial. The consensus is that the magnetic signature of the Verwey transition manifests as a shift of the easy magnetization axis from the [111] to the [100] direction.[37–40] On the other hand, some claim that the two transitions are uncoupled and refer to the slightly higher (130 K) magnetic transition temperature as the "isotropic point" of Fe_3O_4.[41,42] A recent report shows that the small Fe_3O_4 lattice distortion in the c direction may account for the change in magnetic easy axis from cubic [111] to [001] at temperatures less than T_v.[43] This debate is beyond the scope of the present paper. Here, Fe_3O_4 grows in the (111) orientation; therefore, above 120 K, the easy magnetization

[111] axis is perpendicular to the FM easy axis. Thus, above 120 K, there is no magnetic coupling between the two layers, with the consequent absence of EB and M_{Shift} [Fig. 10(a)]. Below 120 K, the easy axis of Fe_3O_4 changes to the [100] direction at $\sim$ 36° with Py, as shown in the inset of Fig. 10(b). Therefore, the nonzero in-plane magnetization component of Fe_3O_4 coincides with the easy in-plane axis of the FM layer, giving rise to EB and M_{Shift} [Fig. 10(b)]. The bilayers studied here are textured, as proved clearly by the x-ray diffraction data, and the cartoons just reflect the magnetic orientation in textured samples.

IV. CONCLUSION

We studied the magnetic properties of FM/V_2O_3 bilayers grown on r-cut sapphire in a variety of configurations. EB in Py/V_2O_3 is accompanied by a large (60%) positive vertical shift in magnetization, indicating the presence of a substantial number of pinned spins. A series of experiments show these effects are related to the formation of a Fe_3O_4 ferrimagnetic interfacial layer. The magnetic signature of the Fe_3O_4 Verwey transition at 120 K coincides with the EB blocking temperature. The large M_{Shift} and EB are produced by interfacial FM coupling due to changes in the Fe_3O_4 magnetic anisotropy. This is the first known observation in which the magnetic signature of the Verwey transition is directly responsible for the presence of EB.

*jdelaventa@physics.ucsd.edu

[1] W. H. Meiklejohn and C. P. Bean, Phys. Rev. **102**, 1413 (1956).

[2] J. Nogués and I. K. Schuller, J. Magn. Magn. Mater. **192**, 203 (1999).

[3] J. C. S. Kools, IEEE Trans. Magn. **32**, 3165 (1996).

[4] C. Tang, J. Appl. Phys. **55**, 2226 (1984).

[5] P. Perna, D. Maccariello, M. Radovic, U. Scotti di Uccio, I. Pallecchi, M. Codda, D. Marré, C. Cantoni, J. Gazquez, M. Varela, S. J. Pennycook, and F. M. Granozio, Appl. Phys. Lett. **97**, 152111 (2010).

[6] J. Ventura, I. Fina, C. Ferrater, E. Langenberg, L. E. Coy, M. C. Polo, M. V. García-Cuenca, L. Fàbrega, and M. Varela, Thin Solid Films **518**, 4692 (2010).

[7] M. Gich, J. Gazquez, A. Roig, A. Crespi, J. Fontcuberta, J. C. Idrobo, S. J. Pennycook, M. Varela, V. Skumryev, and M. Varela, Appl. Phys. Lett. **96**, 112508 (2010).

[8] J. W. Seo, E. E. Fullerton, F. Nolting, A. Scholl, J. Fompeyrine, and J.-P. Locquet, J. Phys. Condens. Matter **20**, 264014 (2008).

[9] C. Rossel, M. Sousa, C. Marchiori, J. Fompeyrine, D. Webb, D. Caimi, B. Mereu, A. Ispas, J. P. Locquet, H. Siegwart, R. Germann, A. Tapponnier, and K. Babich, Microelectron. Eng. **84**, 1869 (2007).

[10] A. Scholl, J. Stöhr, J. Lüning, J. W. Seo, J. Fompeyrine, H. Siegwart, J.-P. Locquet, F. Nolting, S. Anders, E. E. Fullerton, M. R. Scheinfein, and H. A. Padmore, Science **287**, 1014 (2000).

[11] J. B. Goodenough, Prog. Solid State Chem. **5**, 145 (1971).

[12] W. Bruckner, H. Oppermann, W. Reichelt, J. I. Terukow, F. A. Tschudnowski, and E. Wolf, *Vanadium Oxide* (Akademie-Verlag, Berlin, 1983).

[13] M. Imada, A. Fujimori, and Y. Tokura, Rev. Mod. Phys. **70**, 1039 (1998).

[14] F. J. Morin, Phys. Rev. Lett. **3**, 34 (1959).

[15] E. M. Page and S. A. Wass, in *Vanadium: Inorganic and Coordination Chemistry, Encyclopedia of Inorganic Chemistry* (John Wiley & Sons, Chichester, 1994).

[16] D. B. McWhan, J. P. Remeika, T. M. Rice, W. F. Brinkman, J. P. Maita, and A. Menth, Phys. Rev. Lett. **27**, 941 (1971).

[17] B. Sass, C. Tusche, W. Felsch, N. Quaas, A. Weismann, and M. Wenderoth, J. Phys. Condens. Matter **16**, 77 (2004).

[18] B. S. Allimi, S. P. Alpay, C. K. Xie, B. O. Wells, J. I. Budnick, and D. M. Pease, Appl. Phys. Lett. **92**, 202105 (2008).

[19] B. Sass, C. Tusche, W. Felsch, F. Bertran, F. Fortuna, P. Ohresser, and G. Krill, Phys. Rev. B **71**, 014415 (2005).

[20] B. Sass, S. Buschhorn, W. Felsch, D. Schmitz, and P. Imperia, J. Magn. Magn. Mater. **303**, 167 (2006).

[21] A. Maetaki, M. Yamamoto, H. Matsumoto, and K. Kishi, Surf. Sci. **445**, 80 (2000).

[22] The International Centre for Diffraction Data, powder diffraction file No. 00-034-0615.

[23] J. Nogues, C. Leighton, and I. K. Schuller, Phys. Rev. B **61**, 1315 (2000).

[24] H. Ohldag, A. Scholl, F. Nolting, E. Arenholz, S. Maat, A. T. Young, M. Carey, and J. Stöhr, Phys. Rev. Lett. **91**, 017203 (2003).

[25] M. Cheon, Z. Liu, and D. Lederman, J. Appl. Phys. **101**, 09E503 (2007).

[26] C. Zandalazini, P. Esquinazi, G. Bridoux, J. Barzola-Quiquia, H. Ohldag, and E. Arenholz, J. Magn. Magn. Mater. **323**, 2892 (2011).

[27] R. Morales, Z.-P. Li, J. Olamit, K. Liu, J. M. Alameda, and I. K. Schuller, Phys. Rev. Lett **102**, 097201 (2009).

[28] See Supplemental Material at http://link.aps.org/supplemental/10.1103/PhysRevB.85.134447 for three figures showing x-ray diffraction patterns.

[29] E. J. W. Verwey, Nature **144**, 327 (1939).

[30] F. Walz, J. Phys. Condens. Matter **14**, R285 (2002).

[31] S. K. Arora, R. G. S. Sofin, A. Nolan, and I. V. Shvets, J. Magn. Magn. Mater **286**, 463 (2005).

[32] W. B. Mi, J. J. Shen, E. Y. Jiang, and H. L. Bai, Acta Mater. **55**, 1919 (2007).

[33] D. V. Dimitrov, A. S. Murthy, G. C. Hadjipanayis, and C. P. Swann, J. Appl. Phys. **79**, 5106 (1996).

[34] K. W. Lin, P. H. Kol, Z. Y. Guo, H. Ouyang, and J. van Lierop, J. Nanosci. Nanotechnol. **7**, 265 (2007).

[35] B. Mauvernay, L. Presmanes, C. Bonningue, and Ph. Tailhades, J. Magn. Magn. Mater. **320**, 58 (2008).

[36] C. A. Kleint, M. K. Krause, R. Höhne, T. Walter, H. C. Semmelhack, M. Lorenz, and P. Esquinazi, J. Appl. Phys. **84**, 5097 (1998).

[37] R. Prozorov, T. Prozorov, S. K. Mallapragada, B. Narasimhan, T. J. Williams, and D. A. Bazylinski, Phys. Rev. B **76**, 054406 (2007).

[38] M. G. Chaplinea and S. X. Wang, J. Appl. Phys. **97**, 123901 (2005).

[39] R. Aragon, Phys. Rev. B **46**, 5334 (1992).

[40] E. Lima Jr., A. L. Brandl, A. D. Arelaro, and G. F. Goya, J. Appl. Phys. **99**, 083908 (2006).

[41] V. V. Gridin, G. R. Hearne, and J. M. Honig, Phys. Rev. B **53**, 15518 (1996).

[42] F. D. Stacey and S. K. Banerjee, *The Physical Principles of Rock Magnetism* (Elsevier, New York, 1974).

[43] M. S. Senn, J. P. Wright, and J. P. Attfield, Nature **481**, 173 (2012).